**ORIGINAL ARTICLE**

**Open Access**

# GNSS rapid precise point positioning enhanced by low Earth orbit satellites

Ju Hong[1,2], Rui Tu[1,2*], Pengfei Zhang[1,2], Rui Zhang[1], Junqiang Han[1], Lihong Fan[1], Siyao Wang[1] and Xiaochun Lu[1,2]

## Abstract

The Low Earth Orbit (LEO) satellites can be used to effectively speed up Precise Point Positioning (PPP) convergence. In this study, 180 LEO satellites with a global distribution are simulated to evaluate their contribution to the PPP convergence. LEO satellites can give more redundant observations and improve satellite geometric distributions, particularly for a single Global Navigation Satellite System (GNSS). The convergence speed of the PPP float solution using the Global Positioning System (GPS, G) or BeiDou Navigation Satellite System (BDS, C) single system as well as the G/C/Galileo navigation satellite system (Galileo, E)/GLObal NAvigation Satellite System (GLONASS, R) combined system with LEO satellites added is improved by 90.0%, 91.0%, and 90.7%, respectively, with respect to the system without LEO satellites added. We introduced LEO observations to assist GNSS in PPP-AR (Ambiguity Resolution) and PPP-RTK (Real Time Kinematic). The success fix rate of a single system is significantly improved, and the Time-To-First-Fix (TTFF) of G and G/C/E is reduced by 86.4% and 82.8%, respectively, for the PPP-AR solution. We analyzed the positioning performance of LEO satellite assisted G/C/E PPP-RTK in the reference networks of different scales, namely different atmospheric delay interpolation accuracies. The success fix rate of the G/C/E combined system is improved from 86.8 to 94.9%, and the TTFF is reduced by 36.8%, with the addition of LEO satellites in the 57 km reference network. In the 110 km reference network, the success fix rate of the G/C/E combined system is improved from 64.0 to 88.6%, and the TTFF is reduced by 32.1%. GNSS PPP-RTK with adding the LEO satellites in the reference networks of different scales shows obvious improvement because the atmospheric correlation decreases with increasing distance from the reference networks.

**Keywords**  Precise point positioning, Low earth orbit, LEO enhanced global navigation satellite system, Rapid positioning

## Introduction

Precise Point Positioning (PPP) technology has the advantages of limitless operating distance, flexible operation, high precision, and low cost, and is widely used in precise timing, water vapor monitoring, seismic monitoring, precise orbit determination, and other fields (Li et al., 2012, 2015a; Tu et al., 2018; Wright et al., 2012; Zhang & Andersen, 2006; Zumberge et al., 1997). However, the high correlation between ambiguity and hardware delay of satellites and receivers, atmospheric delays, and other factors leads to long convergence time for the float PPP solution, which greatly limits its applications, especially in the fields of rapid and precise positioning and precise orbit determination. The fix of integer ambiguity is of great significance for improving the positioning performance of PPP, and several PPP Ambiguity Resolution (AR) approaches were developed in recent years (Collins et al., 2010; Ge et al., 2008; Laurichesse

*Correspondence:
Rui Tu
turui-2004@126.com
[1] National Time Service Center, Chinese Academy of Sciences, Shu Yuan Road, Xi'an 710600, China
[2] University of Chinese Academy of Sciences, Yu Quan Road, Beijing 100049, China

et al., 2009; Xiao et al., 2018; Zhang & Li (2010). The ambiguity fixing can significantly improve the positioning accuracy and shorten the convergence time of PPP (Ge et al., 2008; Geng et al., 2009). In order to speed up the PPP initialization, some scholars have proposed the methods to improve the performance of PPP using a regional reference network to provide products such as atmospheric delay corrections (Ge et al., 2012; Li et al., 2011; Wübbena et al., 2005; Zhang et al., 2010, 2022a, 2022b, 2014, 2022). The PPP-RTK (Real Time Kinematic) technique using state-space representation, which combines the advantages of PPP and RTK to achieve rapid and high-precision positioning of a single station, has been widely used.

Moreover, many studies showed that multiple Global Navigation Satellite Systems (multi-GNSS) can improve the initialization, accuracy, and continuity of PPP to a certain extent, and shorten the Time To First Fix (TTFF) of AR (Jokinen et al., 2013; Li et al., 2015b, 2015c; Liu et al., 2016; Lou et al., 2016; Tu et al., 2013). With the option of different PPP modes in different application scenarios, the emergence of Low Earth Orbit (LEO) constellation is expected to further improve the performance of multiple PPP modes.

In recent years, LEO constellations have developed rapidly, such as overseas systems of Iridium, oneWeb, SpaceX, and others, and domestic systems of 'Hongyan', 'Hongyun', and 'CentiSpace' (Joerger et al., 2010; Landry et al., 2019; Meng et al., 2018). LEO satellites have the advantages of fast movement speed and strong signal power, which can effectively supplement and improve global Positioning, Navigation, and Timing (PNT) services of GNSS, and have received extensive attention. Iridium and the Iridium NEXT can transmit Satellite Time and Location (STL) signals outside communication services, which can provide PNT services in canyon areas, indoors, and outdoors (Landry et al., 2019; Lawrence et al., 2017). Many scholars tested LEO's contribution to improve GNSS positioning performance in different scenarios (Gao et al., 2021; Ge et al., 2018; Ke et al., 2015; Li et al., 2019a, 2019b, 2022a, 2022b; Tian et al., 2014; Zhao et al., 2020). Ke et al. tested the enhancement performance of LEO for GNSS PPP. Compared with Global Positioning System (GPS), the convergence time of the GPS/LEO combined PPP-AR is reduced by 51.31%, and the positioning accuracy is improved by 14.9%; and the convergence time of GPS/GLObal NAvigation Satellite System (GLONASS) combined PPP-AR is reduced by 3.93%, indicating that LEO satellites contributes more to the convergence speed of PPP than Medium Earth Orbit (MEO) satellites (Ke et al., 2015). Ge et al. used 66 simulated LEO satellites in their tests, and the results showed that LEO enhanced GNSS can reduce the PPP convergence time to 5 min (Ge et al., 2018). The results by Li et al. showed the TTFF of multi-GNSS PPP-AR can be shortened from 7.1 min to 4.8 min, 1.1 min, and 0.7 min with the augmentation of 60-, 192-, and 288-LEO constellations, respectively (Li et al., 2019a). Gao et al., using a constellation of 150 LEO satellites in their experiments, showed that the BeiDou Navigation Satellite System (BDS) and LEO fused PPP convergence time is reduced by about 20 times and decimeter level precision can be achieved in 1 min (Gao et al., 2021). Zhao et al. also investigated the performance of LEO augmented GNSS PPP in harsh environments by setting elevation angle and azimuth. Their results showed that compared with BDS-only, the average TTFF of BDS/GPS, BDS/LEO, BDS/GPS/LEO combination can be shortened from 20.0 min to 10.3 min, 4.8 min, and 4.0 min, respectively, in PPP-AR (Zhao et al., 2020). Li et al. used the simulation data to analyze four LEO constellations with different satellite numbers and scales and the GPS RTK positioning performance for medium and long baselines. The results confirmed that LEO satellites help RTK achieve faster convergence. When the number of LEO satellites was sufficient, the average TTFF for long baselines was reduced by approximately 90% (Li et al., 2019b).

Based on the above analysis, the addition of LEO satellites contributed to a shorter PPP initialization time. However, there are few studies on the effect of LEO on GNSS PPP-RTK positioning performance. Therefore this paper proposes a GNSS ambiguity fix strategy by adding LEO observations and comprehensively evaluates the contribution of LEO to GNSS PPP, PPP-AR, and PPP-RTK positioning performance.

## PPP model

GNSS observations and simulated LEO observations are used in this study. Errors in simulated observations mainly include modelable errors such as satellite clock error, tides error, earth rotation, relativistic effect, tropospheric delay (Saastamoinen model), and phase wind-up. The estimated parameters are the three-dimensional position of a receiver. Therefore, the observation equations for GNSS PPP combined with LEO are as follows:

$$\begin{cases} P_{r,i}^{Q,s} = \rho_r^{Q,s} + cdt_r - cdt^{Q,s} + \gamma_i^{Q,s} I_{r,1}^{Q,s} + M_{w,r}^{Q,s} d_{w,r} + \Theta_{r,i}^{R,s} + d_{r,i} + d_i^{Q,s} + \varepsilon_{P,r,i}^{Q,s} \\ \Phi_{r,i}^{Q,s} = \rho_r^{Q,s} + cdt_r - cdt^{Q,s} - \gamma_i^{Q,s} I_{r,1}^{Q,s} + M_{w,r}^{Q,s} d_{w,r} + \lambda_i^{Q,s} N_{r,i}^{Q,s} + b_{r,i} + b_i^{Q,s} + \varepsilon_{\Phi,r,i}^{Q,s} \\ P_{r,i}^{L,s} = \rho_r^{L,s} - cdt^{L,s} + \varepsilon_{P,r,i}^{L,s} \\ \Phi_{r,i}^{L,s} = \rho_r^{L,s} - cdt^{L,s} + \lambda_i^{L,s} N_{r,i}^{L,s} + \varepsilon_{\Phi,r,i}^{L,s} \end{cases} \tag{1}$$

Here, the subscripts $i$ and $r$ represent the frequency and receiver, respectively, and superscripts s, Q and L represent the specific satellite, GNSS, and LEO, respectively. $P$ and $\Phi$ refer to the code and carrier observations, respectively. $\rho$ denotes the geometric distance between the phase centers of the satellite and the receiver antenna (at signal transmission and reception times). Furthermore, $dt_r$ and $dt^s$ refer to the receiver clock error and satellite clock error; $c$ refers to the speed of light; $M_{w,r}^{Q,s}$ refers to the projection function from the zenith direction of a station to the line-of-sight direction from the station to a satellite; $d_{w,r}$ refers to the troposphere Zenith Wet Delay (ZWD); $I_{r,1}^{Q,s}$ refers to the slant ionosphere delay on the frequency band of $f_1^{Q,s}$; $\gamma_i^{Q,s}$ refers to the frequency-dependent multiplier factor $\gamma_i^{Q,s} = (f_1^{Q,s}/f_i^{Q,s})^2$; $d_{r,i}$ and $d_i^{Q,s}$ refer to the uncalibrated code delays at the satellite and receiver ends, respectively, and $d_{r,i}$ is consistent for band $i$ for all the satellites within the Q system; $b_{r,i}$ and $b_i^{Q,s}$ refer to the uncalibrated phase delays at the satellite and receiver ends, respectively; $\lambda$ refers to the wavelength of the carrier phase; $N$ refers to the integer ambiguity; and $\varepsilon_{P,r,i}^{Q,s}$ and $\varepsilon_{\Phi,r,i}^{Q,s}$ denote the measurement errors, multipath effect, and unmodeled errors of code and carrier phase for GNSS satellites, respectively; $\varepsilon_{P,r,i}^{L,s}$ and $\varepsilon_{\Phi,r,i}^{L,s}$ mainly include the measurement errors of code and carrier phase for LEO satellites, respectively; $\Theta_{r,i}^{R,s}$ refers to the frequency-related code hardware delay for GLONASS satellites using Frequency Division Multiple Access (FDMA) signals. The measurement errors of code and carrier phase for simulated LEO observations are 0.500 m and 0.003 m, respectively.

### Ionosphere-free observations

Ionosphere-Free (IF) code and carrier phase observations are used to eliminate the first-order effect of the ionosphere. This model is used in the tests for PPP float solution and PPP ambiguity fixed solution. If $m$ GNSS satellites and $n$ LEO satellites are observed, using precise orbit and clock error products, the equations of GNSS combined with LEO satellites after performing error correction and reparameterization can be written as:

$$\begin{bmatrix} p_{r,IF}^{Q,1} \\ \varphi_{r,IF}^{Q,1} \\ \vdots \\ p_{r,IF}^{Q,m} \\ \varphi_{r,IF}^{Q,m} \\ p_{r,IF}^{L,1} \\ \varphi_{r,IF}^{L,1} \\ \vdots \\ p_{r,IF}^{L,n} \\ \varphi_{r,IF}^{L,n} \end{bmatrix} = \begin{bmatrix} \boldsymbol{\mu} & \boldsymbol{A} & \boldsymbol{B} & \overline{\boldsymbol{R}}_{IF}^{Q,s} & \boldsymbol{R}_{IF}^{L,s} \end{bmatrix} \begin{bmatrix} \boldsymbol{x} \\ c\bar{d}\bar{t}_r \\ d_{w,r} \\ \lambda_{IF}^{Q,s} \overline{\boldsymbol{N}}_{r,IF}^{Q,s} \\ \lambda_{IF}^{L,s} \boldsymbol{N}_{r,IF}^{L,s} \end{bmatrix} \tag{2}$$



**a** For inclined orbit constellation
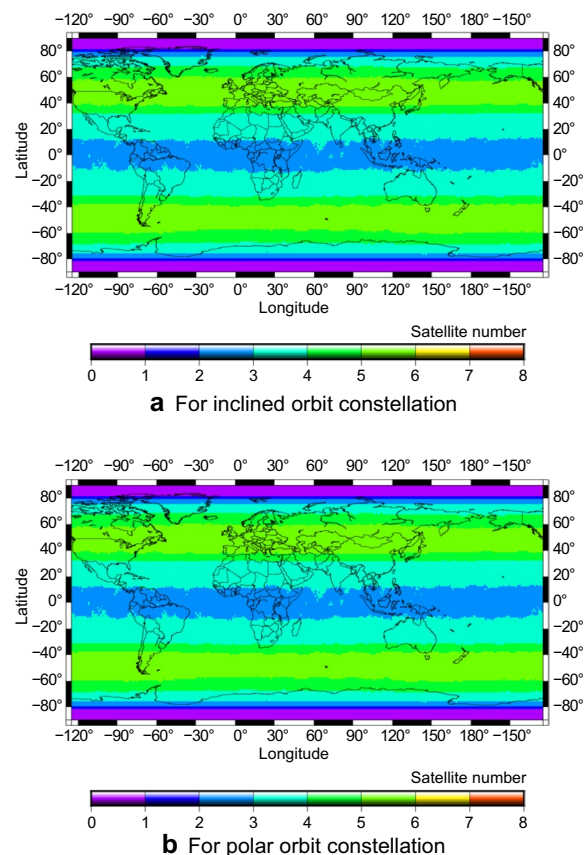


**b** For polar orbit constellation

**Fig. 1** Global distribution of LEO satellites. Subpanels a and b represent the global distributions of LEO satellites in inclined orbit and polar orbit, respectively

In Eq. (2),

$$\begin{cases} c d\bar{t}_r = cdt_r + d_{r,\text{IF}} \\ \lambda_{\text{IF}}^{\text{Q,s}} \overline{N}_{r,\text{IF}}^{\text{Q,s}} = \lambda_{\text{IF}}^{\text{Q,s}} N_{r,\text{IF}}^{\text{Q,s}} + b_{r,\text{IF}} - b_{\text{IF}}^{\text{Q,s}} - d_{r,\text{IF}} + d_{\text{IF}}^{\text{Q,s}} \end{cases}$$
(3)

where $p$ and $\varphi$ represent the observed-minus-computed values of the code and carrier observations, respectively. $\boldsymbol{\mu}$ refers to the unit vector from the receiver to the satellite, and $\boldsymbol{x}$ is the vector of the receiver position increments relative to its prior position. $\boldsymbol{A}$ represents the coefficient matrix of the receiver clock error $c d\bar{t}_r$, the corresponding position is 1 for the GNSS satellite and 0 for the LEO satellite; $\boldsymbol{B}$ represents the coefficient matrix of $d_{w,\text{r}}$, the corresponding position of the GNSS satellite is the projection function, and the corresponding position of LEO is 0; $\overline{\boldsymbol{R}}_{\text{IF}}^{\text{Q,s}}$ refers to the coefficient matrix of ambiguity $\lambda_{\text{IF}}^{\text{Q,s}} N_{r,\text{IF}}^{\text{Q,s}}$ of GNSS satellites,, and the corresponding position is 0 in the code observation equation of GNSS satellite and 1 in the carrier observation equation of GNSS satellite; $\boldsymbol{R}_{\text{IF}}^{\text{L,s}}$ refers to the coefficient matrix of ambiguity $\lambda_{\text{IF}}^{\text{L,s}} N_{r,\text{IF}}^{\text{L,s}}$ of LEO satellites, and the corresponding position is 0 in the code observation equation of the LEO satellite and 1 in the carrier observation equation of the LEO satellite.

## PPP model with atmospheric delay constrain

Atmospheric delays can be extracted by fixing ambiguity through methods at the server end that fix both wide and narrow lane ambiguities based on the ionosphere-free model. The ionospheric delay extracted in a reference network in PPP-RTK is difficult to be separated from the receiver hardware delay and Uncalibrated Phase Delay (UPD) product benchmark (when only satellite UPD products are used), after applying satellite code hardware delay products. Inter-Satellite Difference (SD) ionospheric and the ZWD of tropospheric delay corrections of GNSS satellites are introduced into the Un-Differenced and Un-Combined (UDUC) PPP as virtual observations. This study does not deal with data processing of GLONASS ambiguity fix. Assuming the $f$ th satellite

**Table 1** Adopted models and strategies

| Items | Model and strategies | | |
|---|---|---|---|
| | **PPP float solution** | **PPP-AR solution** | **PPP-RTK solution** |
| Frequency selection | GPS/LEO: L1/L2; BDS-2/BDS-3: B1I/B3I; Galileo: E1/E5a; GLONASS: G1/G2 | GPS/LEO: L1/L2; BDS-3[1]: B1I/B3I; Galileo: E1/E5a; | GPS/LEO: L1/L2; BDS-3: B1I/B3I; Galileo: E1/E5a |
| Sampling interval | 30 s | 5 s | 5 s |
| Estimator | Kalman filtering | Kalman filtering | Kalman filtering |
| Cut-off elevation angle | 7° | Float: 7° Fix: 10° | Float: 7° Fix: 10° |
| Phase ambiguities | Constant estimation | Constant estimation and ambiguities fixed with WL[2]/NL[3] | Server: Constant estimation and ambiguities fixed with WL/NL User: Constant estimation and ambiguities fixed with WL + N1/N2[4] |
| Station coordinates | Estimated as constants in static mode | Estimated as constants in static mode | Server: Constraints, estimated as constants in static mode User: Estimated in dynamic mode |
| Observations | IF observations of carrier phase and code observation | IF observations of carrier phase and code observation | Server: IF observations of carrier phase and code observation User: UCUD phase and code observation |
| Ionospheric delay | Eliminated by IF observations | Eliminated by IF observations | Server: Eliminated by IF observations User: Constraint, Estimated by random walk |
| Tropospheric wet delay | Estimated by random walk NMF mapping function | Estimated by random walk NMF mapping function | (1) Server: Estimated by random walk with NMF[5] mapping function (2) User: Constraint, Estimated by random walk with NMF mapping function |
| Satellite orbit and clock | Precise products | | |
| Satellite and receiver antenna phase center, Tropospheric dry delay, and other modelable errors | Model correction | | |

[1] BDS-3, the third-generation BDS; [2]WL, Wide-Lane; [3]NL, Narrow-Lane; [4]N1/N2, ambiguity at frequency 1/2; [5]NMF, Neill Mapping Function

**Table 2** Numbers of G/C/L/(G/C/R/E) satellites at each station

| Station/system | Satellite numbers of different GNSS | | | |
|---|---|---|---|---|
| | G | C | L | G/C/R/E |
| THU2 | 9.52 | 9.12 | 11.06 | 33.33 |
| ARUC | 8.76 | 11.75 | 7.58 | 29.55 |
| SEYG | 10.16 | 18.84 | 4.75 | 42.96 |

is selected as the reference satellite with Code Division Multiple Access (CDMA) for GNSS and precise orbit and clock error products are used, the observation equations for GNSS combined with LEO after performing error correction and reparameterization are as follows:

equation of GNSS satellite and $-\gamma_i^{Q,s}$ in the carrier observation equation of the GNSS satellite, the corresponding position is 0 for the LEO satellite. $\overline{R}_1^{Q,s}$ and $\overline{R}_2^{Q,s}$ refer to the coefficient matrix of ambiguity $\lambda_1^{Q,s}\overline{N}_{r,1}^{Q,s}$ and $\lambda_2^{Q,s}\overline{N}_{r,2}^{Q,s}$ of GNSS satellites, respectively, and the corresponding position is 0 in the code observation equation of the GNSS satellite and 1 in the carrier observation equation of the GNSS satellite; $R_1^{L,s}$ and $R_2^{L,s}$ refer to the coefficient matrix of ambiguity $\lambda_1^{L,s}\overline{N}_{r,1}^{L,s}$ and $\lambda_2^{L,s}\overline{N}_{r,2}^{L,s}$ of LEO satellites, respectively, and the corresponding position is 0 in the code observation equation of the LEO satellite and 1 in the carrier observation equation of the LEO satellite; $D$

$$
\begin{bmatrix}
p_{r,1}^{Q,1} \\
\varphi_{r,1}^{Q,1} \\
\vdots \\
p_{r,2}^{Q,m} \\
\varphi_{r,2}^{Q,m} \\
p_{r,1}^{L,1} \\
\varphi_{r,1}^{L,1} \\
\vdots \\
p_{r,2}^{L,n} \\
\varphi_{r,2}^{L,n} \\
\Delta\overline{I}_1^{(Q,1),(Q,f)} \\
\vdots \\
\Delta\overline{I}_1^{(Q,m-1),(Q,f)} \\
\overline{d}_{w,r}
\end{bmatrix}
=
\begin{bmatrix}
\boldsymbol{\mu} & \boldsymbol{A} & \boldsymbol{B} & \boldsymbol{K} & \overline{\boldsymbol{R}}_1^{Q,s} & \overline{\boldsymbol{R}}_2^{Q,s} & \boldsymbol{R}_1^{L,s} & \boldsymbol{R}_2^{L,s} & \boldsymbol{D} \\
\boldsymbol{O} & \boldsymbol{O} & \boldsymbol{O} & \overline{\boldsymbol{K}} & \boldsymbol{O} & \boldsymbol{O} & \boldsymbol{O} & \boldsymbol{O} & \boldsymbol{O} \\
\boldsymbol{O} & \boldsymbol{O} & \boldsymbol{T} & \boldsymbol{O} & \boldsymbol{O} & \boldsymbol{O} & \boldsymbol{O} & \boldsymbol{O} & \boldsymbol{O}
\end{bmatrix}
\begin{bmatrix}
\boldsymbol{x} \\
cd\overline{t}_r \\
d_{w,r} \\
\boldsymbol{I}_{r,1}^{Q,s} \\
\lambda_1^{Q,s}\overline{\boldsymbol{N}}_{r,1}^{Q,s} \\
\lambda_2^{Q,s}\overline{\boldsymbol{N}}_{r,2}^{Q,s} \\
\lambda_1^{L,s}\boldsymbol{N}_{r,1}^{L,s} \\
\lambda_2^{L,s}\boldsymbol{N}_{r,2}^{L,s} \\
d_{r,12}^{DCB}
\end{bmatrix}
\tag{4}
$$

In Eq. (4),

$$
\begin{cases}
d_{r,12}^{DCB} = d_{r,1} - d_{r,2} \\
\lambda_i^{Q,s}\overline{N}_{r,i}^{Q,s} = \lambda_i^{Q,s}N_{r,i}^{Q,s} + b_{r,i} - b_i^{Q,s} - d_{r,IF} + d_{IF}^{Q,s}
\end{cases}
\tag{5}
$$

where $\boldsymbol{K}$ represents the coefficient matrix of the slant ionospheric delay $I_{r,1}^{Q,s}$, with $\gamma_i^{Q,s}$ in code observation

represents the coefficient matrix of the receiver differential code hardware delay $d_{r,12}^{DCB}$, the corresponding position is $-\left(f_2^{Q,s}\right)^2/[\left(f_1^{Q,s}\right)^2 - \left(f_2^{Q,s}\right)^2]$ in the code observation equation on frequency 1 and $-\left(f_1^{Q,s}\right)^2/[\left(f_1^{Q,s}\right)^2 - \left(f_2^{Q,s}\right)^2]$ in the code observation equation on frequency 2 of the GNSS satellite. $\overline{K}$

**Table 3** PDOP values of different systems at each station

| Station/system | PDOP values of different GNSS | | | | | |
|---|---|---|---|---|---|---|
| | G | G/L | C | C/L | G/C/R/E | G/C/R/E/L |
| THU2 | 2.16 | 1.28 | 2.32 | 1.33 | 0.98 | 0.80 |
| ARUC | 1.84 | 1.23 | 1.80 | 1.12 | 0.96 | 0.80 |
| SEYG | 1.73 | 1.37 | 1.22 | 1.05 | 0.78 | 0.73 |

represents the coefficient matrix of the SD iono-sphere delay for GNSS with −1 for the reference satellites and 1 for the other satellites. $T$ represents the coefficient matrix of $d_{w,r}$ with 1, and $O$ represents the zero matrix. The GPS, GLONASS, Galileo navigation satellite system (Galileo), BDS, and LEO are usually represented by 'G', 'R', 'E', 'C', and 'L', respectively.

## Experimental results and analysis

The LEO constellation design is the key to the establishment of satellite systems. Many scholars simulated different LEO constellations for verifying their augmentation performances (Han et al., 2020; Liu et al., 2022; Ma et al., 2020). The enhancement effect of LEO on GNSS depends on the number and the geometric distribution of satellites. We simulated two commonly used low-orbit constellations, namely, inclined orbit constellations and polar orbit constellations, which have a global coverage. There are 80 satellites in six polar orbits with an orbital inclination of 90° and 100 satellites in 10 inclined orbits with an orbital inclination of 60°. The orbital altitude of LEO satellites is 1000 km. The globe was divided into 1°×1° grids. The global distributions of LEO satellites in inclined orbit and polar orbit are shown in Fig. 1(a)
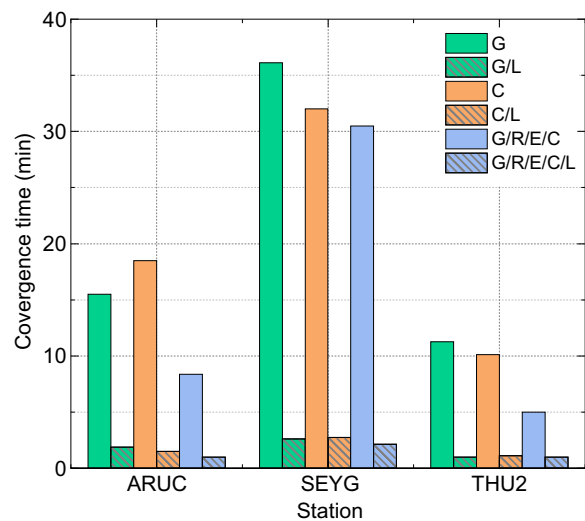


**Fig. 3** Convergence time of GNSS/LEO PPP float solution

and (b) respectively, which use the median of the visible satellites in every 30 s of a day with a cut-off angle of 7°. The coverage for the inclined orbit constellation can reach approximately latitude 80°, and the largest number
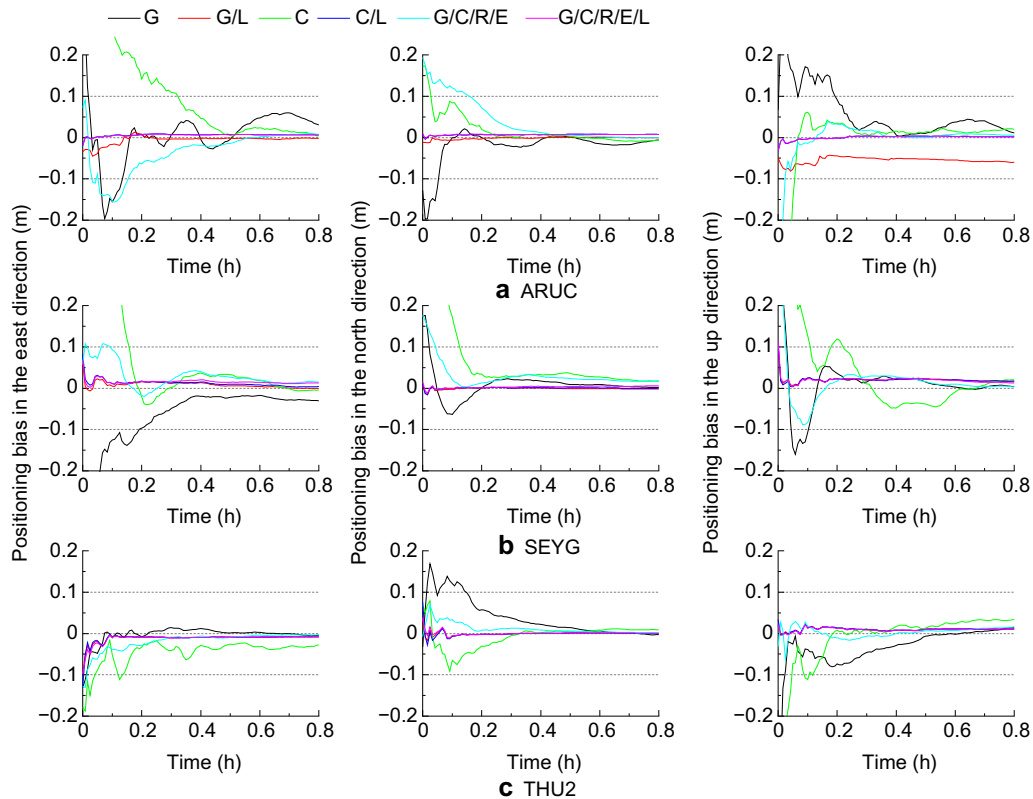


**Fig. 2** Positioning bias of GNSS/LEO PPP float solution at three stations. Subpanels **a**–**c** represent the positioning biases of ARUC, SEYG, and THU2 stations, respectively

of satellites is in the region of latitudes 30°–60°, which shows relatively uniform satellite coverage. While the polar orbit constellations give the largest number of satellites in the region of north and south latitudes higher than 60°, achieving coverage and service in high latitude and polar regions.

The distribution of the simulated LEO constellation and its effect on GNSS positioning are analyzed below. LEO satellite observations are used to assist the GNSS PPP-AR and PPP-RTK solutions. The adopted models and strategies are shown in Table 1.



**Fig. 4** Station distribution for the test (The blue origins and the red asterisks represent reference stations and user stations, respectively)

## PPP float solution

The number and distribution of satellites vary in different latitudes, which affect the positioning results. Hence, three typical stations in high, middle, and low latitudes are selected to analyze the enhancement effect of LEO on the GNSS float solution. The three stations and their geographical locations are THU2 (76.5° N, 68.8° W), ARUC (40.3° N, 44.1° E), and SEYG (4.7° S, 74.5° E). Tables 2 and 3 show the number of satellites and PDOP values of each system at the three stations on January 1, 2022. The average numbers of LEO satellites visible at the three stations are about 11, 8, and 5 respectively. The polar orbit constellation makes the largest number of LEO satellites visible at the high-latitude station THU2. The geometric distribution of satellites in a single system is greatly improved with LEO added, particularly for the stations with a poor geometric distribution of satellites. The addition of LEO satellites improved PDOP of G/C/R/E though the four systems have more satellites with good distribution, which facilitates the rapid solution of PPP.

To further analyze the convergence speed with the addition of LEO satellites, PPP is conducted for every 6 h session of the single-day data at the three stations. The positioning bias at a certain period of time and the convergence speed of (G/C/R/E)/C/G without and with LEO satellites are shown in Figs. 2 and 3, respectively. The convergence condition is defined as the positioning biases of horizontal and vertical components maintained within 10 cm. With adding LEO satellites, the convergence speed of (G/C/R/E)/C/G at the three stations is much faster. With LEO added, GPS/BDS/GNSS solutions
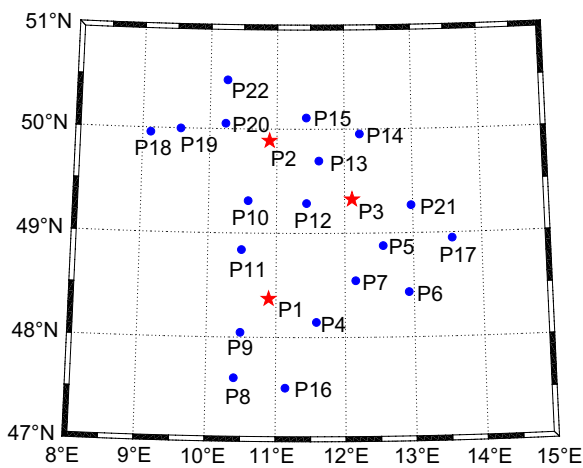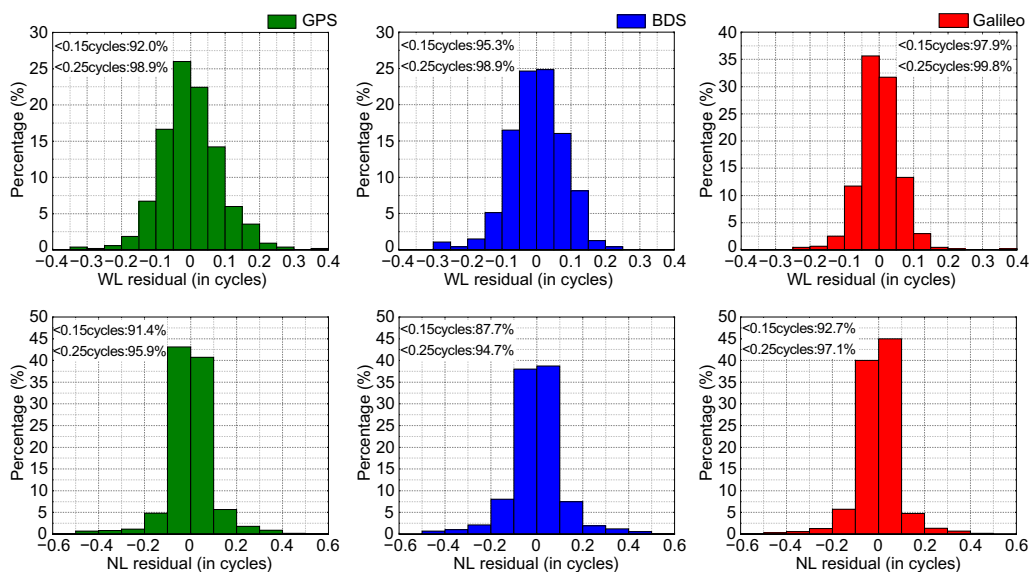


**Fig. 5** Distribution of WL and NL UPD posteriori residuals. The upper part represents WL posteriori residuals of GPS/BDS/Galileo from left to right, and the lower part represents the NL posteriori residual of GPS/BDS/Galileo from left to right
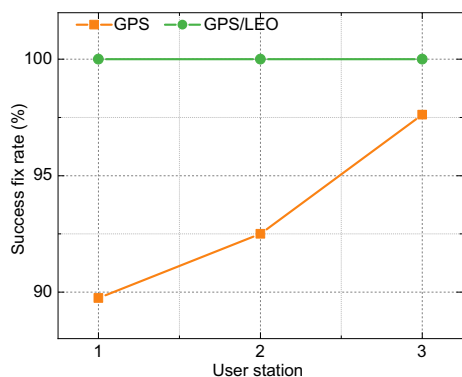
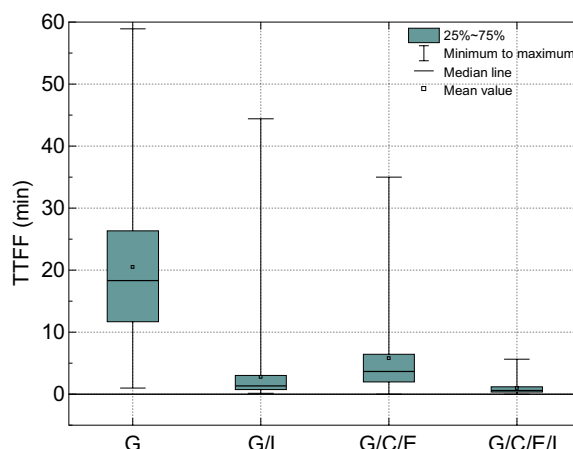**Fig. 6** The success fix rate of G/(G/L) at each station



**Fig. 7** TTFF distribution of in PPP-AR solution

**Table 4** The success fix rate and mean TTFF of different systems in PPP-AR solution

| System | Success fix rate (%) | TTFF (min) |
|---|---|---|
| G | 93.4 | 20.5 |
| G/L | 100 | 2.8 |
| G/C/E | 100 | 5.8 |
| G/C/E/L | 100 | 1.0 |

reached the convergence conditions in 1.9 min, 1.8 min, and 1.3 min, respectively, and the convergence speed is increased by 90.0%, 91.0%, and 90.7%, respectively.

**PPP-AR solution**

Correct ambiguity fixing is of great significance for improving positioning accuracy, and the speed of fixed ambiguity is closely related to the floating solution. As shown in the previous section, the speed of floating solution is significantly improved with the LEO satellite. This section focuses on the analysis of the effect of the LEO satellites on the improvement of the TTFF and success fix rate for GNSS PPP-AR. The PPP is performed every half an hour for 1 h with each solution time and therefore each station has 47 PPP solutions a day. The G and G/C/E combined systems are selected to analyze the effect of adding LEO satellites on the AR for a single system as well as multi-GNSS. The test in this section adopted the data from European stations on June 21, 2022. The distribution of stations is shown in Fig. 4. 19 reference stations are used to calculate the UPD (fraction part), which is represented by the blue dots in Fig. 4, and three user stations are represented by the red asterisk. The influence of addition LEO satellites on the G/(G/C/E) ambiguity-fixed solution is analyzed based on the success fix rate and TTFF. Here, the success fixed solution is defined as the periods of TTFF less than 1 h, and the success fix rate
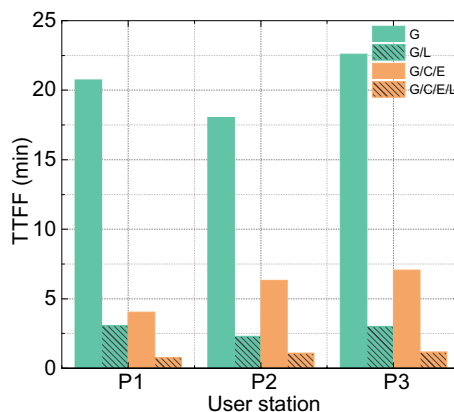


**Fig. 8** The mean TTFF of each station in PPP-AR

is defined as the ratio of the number with success fixed solutions to the total number of solutions. The TTFF is defined as the start time when a fixed solution of less than 10 cm in the horizontal and vertical components is achieved and lasts for 10 consecutive epochs.

The method of ambiguity resolution of UPD parameters is used in the test, so the UPD product is an important premise of PPP ambiguity resolution. The Wide-Lane (WL) UPDs are very stable owing to their long wavelength feature and insensitivity to the errors of measurement, while the Narrow-Lane (NL) UPDs are not as stable as the WL UPD (Zhang & Li, 2013). The WL UPDs are estimated for one day, while the NL UPDs are estimated every 15 min (Ge et al., 2008; Zhang & Li, 2013). The posteriori residuals will reflect the quality of the UPD products. The RMS distributions of the posteriori residuals of the GPS/BDS/Galileo WL and NL UPDs are shown in Fig. 5. The WL and NL UPD residuals of more than 94% for the three systems are less than 0.25
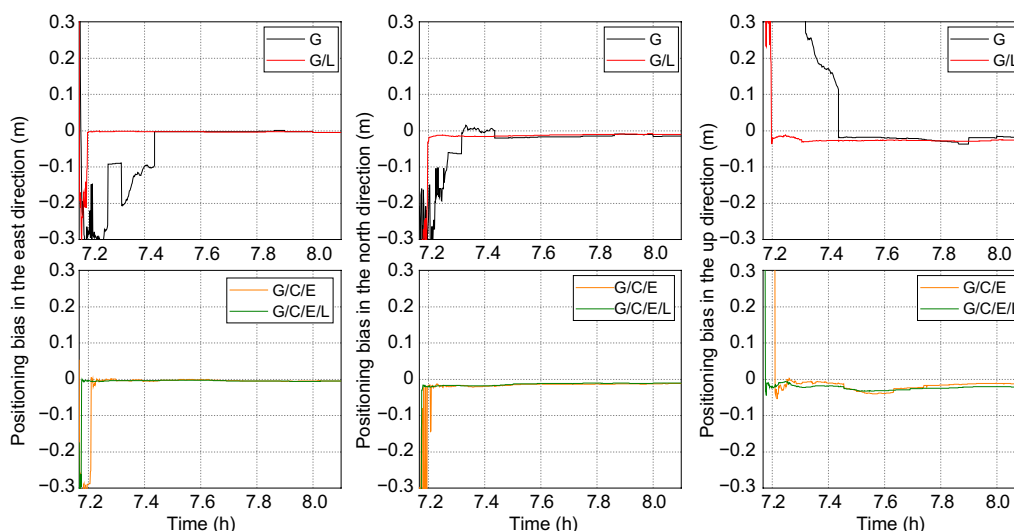
**Fig. 9** Positioning biases of different systems in PPP-AR solution
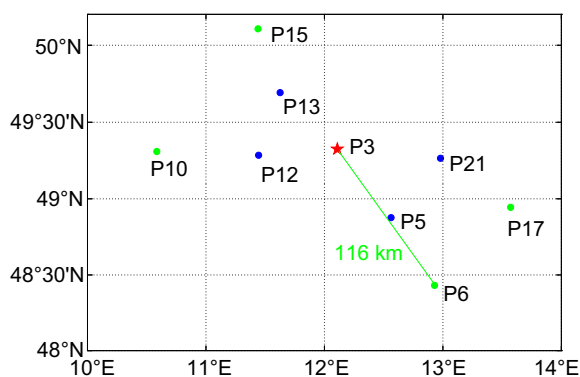


**Fig. 10** Station distribution in PPP-RTK tests (The dots and the asterisk represent reference stations and user station, respectively. The blue dots and green dots represent the reference stations located 57 km and 110 km, respectively, away from user station)

cycles. The means of the posteriori residuals are close to zero and the RMS values are 0.098 cycles, 0.113 cycles, and 0.089 cycles in NL and 0.086 cycles, 0.059 cycles, and 0.077 cycles in WL UPDs, respectively.

Due to the smaller number and poor geometric distribution of the satellites for a single system, the convergence speed of the floating solution for a single system may be slow, which leads to that the ambiguity cannot be fixed successfully in a short time. As shown in Fig. 6 and Table 4, the success fix rates for GPS at the three stations are about 90%. While with the addition of LEO satellites, the success fix rate reaches 100%.

The systems G/C/E and G/C/E/L can fix integer ambiguity within 1 h. However, the TTFF of G/C/E/L is within 5 min, much faster than that of G/C/E, as shown in Fig. 7.

With the addition of LEO satellites, the TTFFs of a single system and multiple systems are further reduced, and the TTFF at each station is almost the same, as shown in Fig. 8. As is shown in Table 4, with LEO satellites added to the G and (G/C/E), the TTFFs are reduced by 86.4% and 82.8%, respectively. The positioning biases with adding LEO are shown in Fig. 9 for G/(G/L)/(G/C/E)/(G/C/E/L) in the east (*E*)/north (*N*)/up (*U*) component for a certain period. The addition of the LEO satellites can significantly improve the convergence speed and positioning bias.

## PPP-RTK solution

PPP-RTK enables rapid ambiguity resolution by exploiting the precise atmospheric delay provided by a regional network. This section focuses on the analysis of TTFF and success fix rate in reference networks of different scales. The above regional network data are selected to analyze the effect of LEO on the performance of G/C/E PPP-RTK using two kinds of reference networks including the medium-long scale with an average distance of 57 km and the larger scale with an average distance of 110 km between user stations and reference stations. The station distributions are shown in Fig. 10. The data acquisition was done in 1:00–23:40 UTC (Coordinated Universal Time), June 21, 2022. The PPP-RTK is performed every 5 min during the experiment with a total of 272 data sets with 5 min each. The atmospheric delays at the serve end were modeled using the observations from a single epoch with a sampling interval of 5 s. TTFF in the horizontal components is defined as the time required for the ratio value to be greater than 2, and the positioning bias of horizontal components to be less than 5 cm
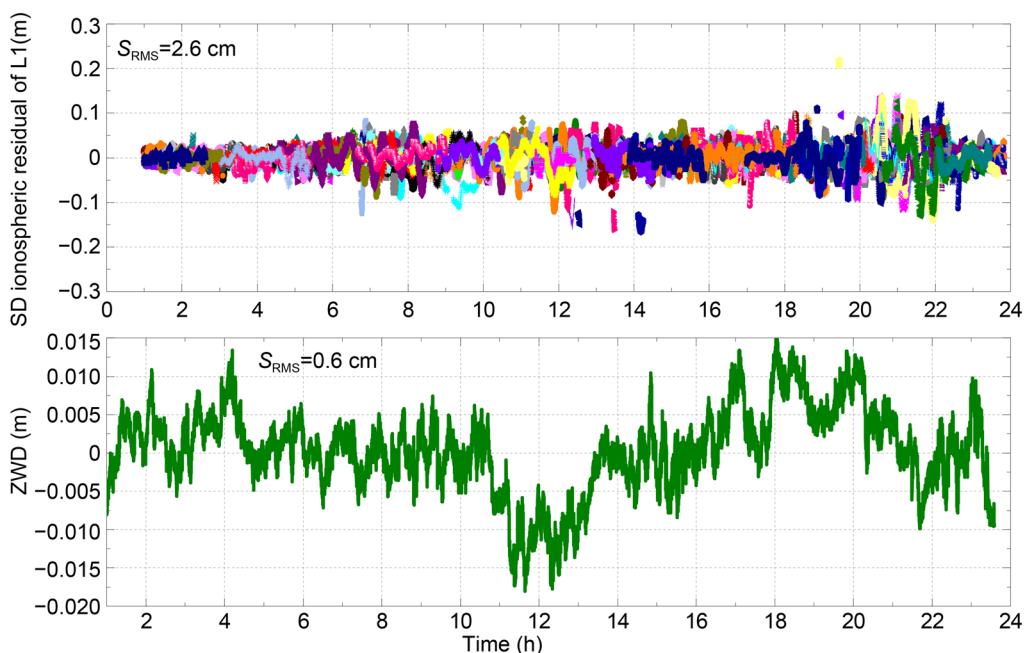
**Fig. 11** SD ionospheric interpolation residuals and zenith wet delay interpolation residuals of G/C/E in the 57 km reference network

**Table 5** The success fix rate and mean TTFF in the 57 km reference network

| System | Evaluation method | Success fix rate (%) | TTFF (s) |
|---|---|---|---|
| G/C/E | Horizontal | 89.0 | 13.25 |
| G/C/E/L | Horizontal | 95.6 | 9.33 |
| G/C/E | Three-dimensional | 86.8 | 16.08 |
| G/C/E/L | Three-dimensional | 94.9 | 10.16 |



**Fig. 12** The cumulative distribution of (G/C/E)/(G/C/E/L) TTFF in horizontal and three-dimensional components in the 57 km reference network

for 10 consecutive epochs. TTFF in the three-dimensional components is defined as the time required for the ratio value to be greater than 2, the positioning bias of horizontal components to be less than 5 cm, and the vertical component to be less than 10 cm for 10 consecutive epochs. Here, the successfully fixed solution is defined as the periods of TTFF less than 5 min, and the success fix rate is defined as the ratio of the number with successfully fixed solutions to the total number of solutions.

**The 57 km reference network**
This network means the reference stations are 50 km away from the user station. Stations P5/P12/P13/P21 are the reference stations and station P3 the user station. Figure 11 shows the G/C/E SD ionospheric residuals and tropospheric zenith wet delay residuals with Root Mean Square (RMS) $S_{RMS}$ values of 2.6 and 0.6 cm, respectively.
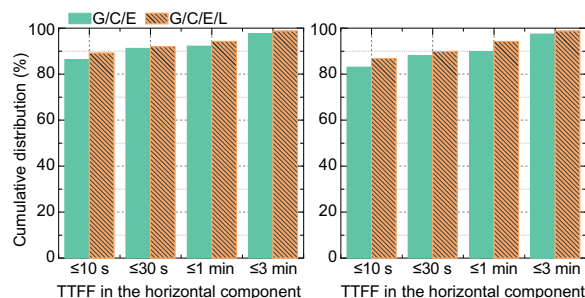
The PPP-RTK technology intends to enhance the ambiguity resolution by introducing external information on atmospheric delay. The mean TTFF and success fix rate in the horizontal components as well as in the three-dimensional components are shown in Table 5. The success fix rates are 89.0% and 86.8% in the horizontal and three-dimensional components in the G/C/E combined system, respectively, and improved to 95.6% and 94.9% with the assistance of LEO satellites. The mean TTFFs in the horizontal and three-dimensional components for the G/C/E combined system are 13.25 s and 16.08 s, respectively, which are reduced to 9.33 s and 10.16 s, with an improvement by 29.6% and 36.8%. Further statistics of
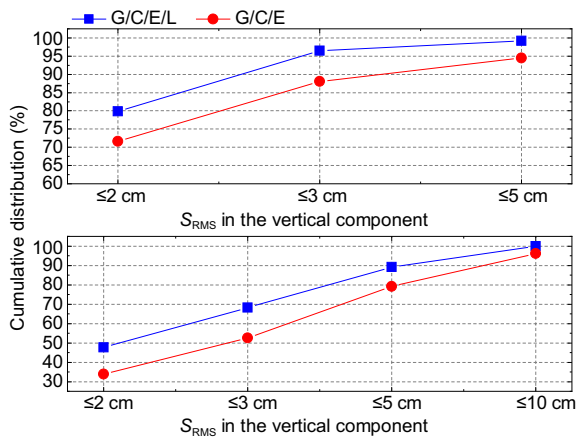
**Fig. 13** The cumulative distribution of the RMSs in horizontal and vertical components in the 57 km reference network

**Table 6** The success fix rate and mean TTFF in the 110 km reference network

| System | Evaluation method | Success fix rate (%) | TTFF (s) |
|---|---|---|---|
| G/C/E | Horizontal | 69.1 | 35.6 |
| G/C/E/L | Horizontal | 89.3 | 26.0 |
| G/C/E | Three-dimensional | 64.0 | 41.8 |
| G/C/E/L | Three-dimensional | 88.6 | 28.4 |

TTFF cumulative distributions in each system are shown in Fig. 12. With the addition of LEO satellites, the TTFFs within 10 s/30 s/1 min/3 min are all better, and successful ambiguity fixing in the three-dimensional components is achieved in 10 s for 86.8% of the periods, in 30 s for 89.9%, and in 1 min for 94.2%.

The addition of LEO satellites can further speed up the ambiguity resolution of multiple systems, and the positioning accuracy in a short time is evaluated below. The RMS cumulative distributions of positioning bias in
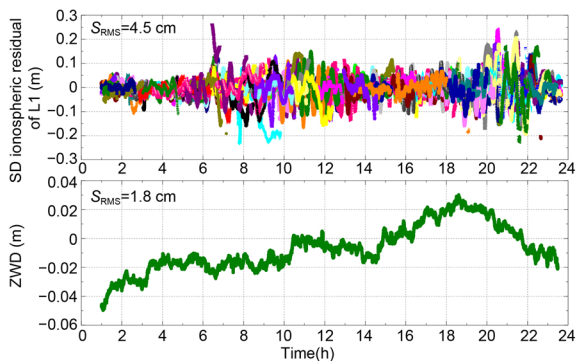


**Fig. 14** SD ionospheric interpolation residuals and zenith wet delay interpolation residuals of G/C/E in the 110 km reference network
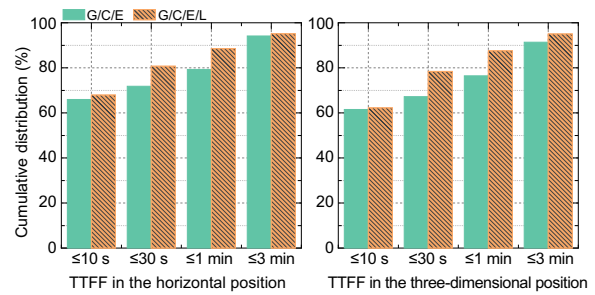


**Fig. 15** The cumulative distribution of (G/C/E)/(G/C/E/L) system TTFF in horizontal and three-dimensional components in the 110 km reference network
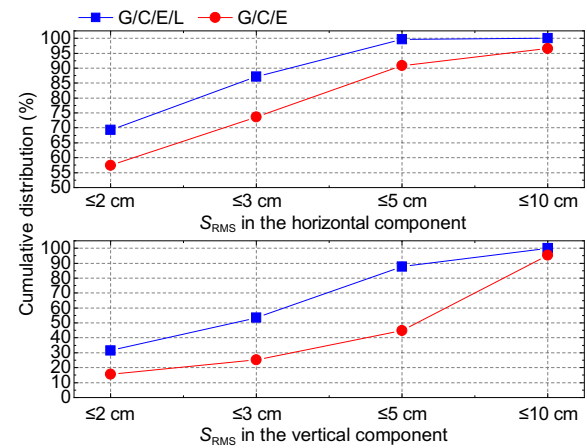


**Fig. 16** The cumulative distribution of RMSs in horizontal and vertical components in the 110 km reference network

horizontal and vertical components after ambiguity fixing are shown in Fig. 13. With LEO satellites added, the $S_{RMS}$ values are less than 2 cm and 3 cm for 79.8% and 96.5% of the periods with successful ambiguity fixing, respectively, and larger than 5 cm in the horizontal components for some periods. The $S_{RMS}$ values are less than 3 cm and 5 cm for 68.2% and 89.1% of the convergence periods, respectively, and less than 10 cm in all periods in the vertical component for a 5 min solution duration.

### The 110 km reference network

This network means the reference stations are 110 km away from the user station. Stations P6/P10/P15/P17 are the reference stations and station P3 the user station. Figure 14 shows the G/C/E SD ionospheric residuals and tropospheric zenith wet delay residuals with RMS values of 4.5 and 1.8 cm, respectively.

The mean TTFF and success fix rate in the horizontal components as well as in the three-dimensional components are shown in Table 6. The success fix rates are 69.1% and 64.0% in the horizontal and three-dimensional

components in the G/C/E combined system, and improved to 89.3% and 88.6%, respectively with the addition of LEO satellites. The mean TTFFs in the horizontal and three-dimensional components for the G/C/E combined system are 35.6 and 41.8 s, respectively, which are reduced to 26.0 s and 28.4 s with an improvement by 27% and 32.1%, respectively, with the addition of LEO satellites. Further statistics of TTFF cumulative distributions in each system are shown in Fig. 15. With the addition of LEO satellites, the TTFFs within 10 s/30 s/1 min/3 min are all better, and the ambiguity fixing is achieved in 10 s for 62.2% in three dimensions, 30 s for 78.4% of epochs, and 1 min for 87.6% of epochs. The horizontal and vertical RMS cumulative distributions of positioning bias after ambiguity fixing are shown in Fig. 16. With LEO satellite added, the $S_{RMS}$ values of positioning bias are less than 2 cm and 5 cm for 69.3% and 99.6% of the convergence periods, respectively, and larger than 5 cm in the horizontal components for some periods. The $S_{RMS}$ values are less than 3 cm and 5 cm for 53.5% and 87.6% of the periods with successful ambiguity fixing, respectively, and less than 10 cm in all periods in the vertical component for a 5 min solution duration.

## Conclusion

Because LEO satellites have low orbits and high moving speeds, their addition to GNSS can increase the geometric diversity of visible satellites and achieve rapid PPP solutions. Herein, we tested the positioning performances of LEO aided GNSS PPP float solution, PPP-AR, and PPP-RTK using simulated LEO data.

The effects of LEO on GNSS are related to the number and geometric distribution of satellites. First, three stations in high, middle, and low latitudes were selected for the PPP float solution test. The results show that the addition of LEO satellites improved the geometric distribution of satellites, particularly for a single system. With the addition of LEO, the G/C/(G/C/E/R) PPP float solutions reached convergence conditions in 1.9 min, 1.8 min, and 1.3 min, with convergence speed increased by 90.0%, 91.0%, and 90.7%, respectively. Correct ambiguity fixing is of great significance for speeding up the convergence and improving positioning accuracy. A European regional reference network was selected to test the effects of LEO on the G and G/C/E in PPP-AR. Using LEO observations to assist GNSS PPP-AR solutions, the success fix rate of G is increased from 93.4 to 100%. Also the TTFFs of G and G/C/E are improved by 86.4% and 82.8%, respectively. Finally, the European reference network was selected to analyze the positioning performance of the LEO-assisted G/C/E PPP-RTK in the reference networks of different scales. With the addition of LEO satellites, the success fix rates of the G/C/E which evaluated

by the positioning biases in horizontal and three-dimensional components are increased from 89.0% and 86.8% to 95.6% and 94.9%, respectively, and the TTFF reduced from 13.25 s and 16.08 s to 9.33 s and 10.16 s with an improvement by 29.6% and 36.8% in the reference network with an average distance of 57 km between a user station and reference stations, respectively. Within the reference network with an average distance of 110 km between a user station and reference stations, the success fix rates of the G/C/E evaluated by the positioning biases in horizontal and three-dimensional components are increased from 69.1% and 64.0% to 89.3% and 88.6%, respectively, and the TTFF reduced from 35.6 s and 41.8 s to 26.0 s and 28.4 s with an improvement by 27% and 32.1%, respectively.

**Author contributions**
JH and RT provided the initial idea for this work and wrote this manuscript; PZ, RZ, LF, JH, SW and XL contributed to the analyses of results and the discussions. All authors read and approved the final manuscript.

**Availability of data and materials**
The data generated or analyzed during this study are available from the corresponding author on reasonable request.

## Declarations

**Competing interests**
The authors declare that they have no competing interests.

**References**
Collins, P., Bisnath, S., Lahaye, F., & Héroux, P. (2010). Undifferenced GPS ambiguity resolution using the decoupled clock model and ambiguity datum fixing. *Navigation, 57*(2), 123–135.

Gao, W., Zhang, G., Liu, C., Lu, J., Wang, W., Chen, Y., Li, M., & Lv, F. (2021). Research and simulation of LEO-based navigation augmentation. *Scientia Sinica Physica, Mechanica & Astronomica, 51*, 019506.

Ge, H., Li, B., Ge, M., Zang, N., Nie, L., Shen, Y., & Schuh, H. (2018). Initial assessment of precise point positioning with LEO enhanced global navigation satellite systems (LeGNSS). *Remote Sensing, 10*(7), 984–999.

Ge, M., Doua, J., Li, X., Ramatschi, M., & Wickert, J. (2012). A novel real-time precise positioning service system: Global precise point positioning with regional augmentation. *Journal of Global Positioning Systems, 11*(1), 2–10.

Ge, M., Gendt, G., Rothacher, M., Shi, C., & Liu, J. (2008). Resolution of GPS carrier-phase ambiguities in Precise Point Positioning (PPP) with daily observations. *Journal of Geodesy, 82*(7), 389–399.

Geng, J., Teferle, F. N., Shi, C., Meng, X., Dodson, A. H., & Liu, J. (2009). Ambiguity resolution in precise point positioning with hourly data. *GPS Solutions, 13*(4), 263–270.

Han, Y., Wang, L., Fu, W., Zhou, H., Li, T., Xu, B., & Chen, R. (2020). LEO navigation augmentation constellation design with the multi-objective

optimization approaches. *Chinese Journal of Aeronautics, 34*(4), 265–278.

Joerger, M., Gratton, L., Pervan, B., & Cohen, C. E. (2010). Analysis of iridium-augmented GPS for floating carrier phase positioning. *Navigation, 57*(2), 137–160.

Jokinen, A., Feng, S., Schuster, W., Ochieng, W., Hide, C., & Hill, T. M. C. (2013). GLONASS aided GPS ambiguity fixed precise point positioning. *Journal of Navigation, 66*(03), 399–416.

Ke, M., Lv, J., Chang, J., Dai, W., Tong, K., & Zhu, M. (2015). Integrating GPS and LEO to accelerate convergence time of precise point positioning. In *Proceedings of 2015 international conference on wireless communications & signal proceeding (WCSP)*.

Landry, R. J., Nguyen, A. Q., Rasaee, H., Amrhar, A., Fang, X., & Benzerrouk, H. (2019). Iridium next LEO satellites as an alternative PNT in GNSS denied environments—Part 1. *Inside GNSS, 14*(3), 56–65.

Laurichesse, D., Mercier, F., Berthias, J. P., Broca, P., & Cerri, L. (2009). Integer ambiguity resolution on undifferenced GPS phase measurements and its application to PPP and satellite precise orbit determination. *Navigation, 56*(2), 135–149.

Lawrence, D., Cobb, H. S., Gutt, G., O'Connor, M., Reid, T. G. R., Walter, T., & Whelan, D. (2017). Innovation: Navigation from LEO 2017. Retrieved June 30, 2017, from https://www.gpsworld.com/innovation-navigation-from-leo/

Li, X., Zhang, X., & Ge, M. (2011). Regional reference network augmented precise point positioning for instantaneous ambiguity resolution. *Journal of Geodesy, 85*(2), 151–158.

Li, X., Zhang, X., & Li, P. (2012). PPP for rapid precise positioning and orbit determination with zero-difference integer ambiguity fixing. *Chinese Journal of Geophysics, 55*(3), 833–840. (**in Chinese**).

Li, X., Ge, M., Doua, J., & Wickert, J. (2014). Real-time precise point positioning regional augmentation for large GPS reference networks. *GPS Solutions, 18*(1), 61–71.

Li, X., Zus, F., Lu, C., Dick, G., Ning, T., Ge, M., Wickert, J., & Schuh, H. (2015a). Retrieving of atmospheric parameters from multi-GNSS in real time: Validation with water vapor radiometer and numerical weather model. *Journal of Geophysical Research: Atmospheres, 120*(14), 7189–7204.

Li, X., Ge, M., Dai, X., Ren, X., Fritsche, M., Wickert, J., & Schuh, H. (2015b). Accuracy and reliability of multi-GNSS real-time precise positioning: GPS, GLONASS, BeiDou, and Galileo. *Journal of Geodesy, 89*(6), 607–635.

Li, X., Zhang, X., Ren, X., Fritsche, M., Wickert, J., & Schuh, H. (2015c). Precise positioning with current multi-constellation global navigation satellite systems: GPS, GLONASS, Galileo and BeiDou. *Scientific Reports, 5*(1).

Li, X., Li, X., Ma, F., Yuan, Y., & Zhang, X. (2019a). Improved PPP ambiguity resolution with the assistance of multiple LEO constellations and signals. *Remote Sensing, 11*(4), 408.

Li, X., Lv, H., Ma, F., Li, X., Liu, J., & Jiang, Z. (2019b). GNSS RTK positioning augmented with large LEO constellation. *Remote Sensing, 11*(3), 228.

Li, X., Wang, B., Li, X., Huang, J., Lyu, H., & Han, X. (2022a). Principle and performance of multi-frequency and multi-GNSS PPP-RTK. *Satellite Navigation, 3(1)*, 7.

Li, M., Xu, T., Guan, M., Gao, F., & Jiang, N. (2022b). LEO-constellation-augmented multi-GNSS real-time PPP for rapid reconvergence in harsh environments. *GPS Solutions, 26*.

Liu, T., Yuan, Y., Zhang, B., Wan, N., Tan, B., & Chen, Y. (2016). Multi-GNSS precise point positioning (MGPPP) using raw observations. *Journal of Geodesy, 91*, 1–16.

Liu, J., Hao, J., Yang, Y., Xu, Z., Liu, W., & Wu, R. (2022). Design optimisation of low earth orbit constellation based on BeiDou Satellite Navigation System precise point positioning. *IET Radar, Sonar & Navigation., 16*(8), 1241–1252.

Lou, Y., Zheng, F., Gu, S., Wang, C., Guo, H., & Feng, Y. (2016). Multi-GNSS precise point positioning with raw single-frequency and dual-frequency measurement models. *GPS Solutions, 20*(4), 849–862.

Ma, F., Zhang, X., Li, X., Chen, J., Guo, F., Hu, J., & Pan, L. (2020). Hybrid constellation design using a genetic algorithm for a LEO-based navigation augmentation system. *GPS Solutions, 24*, 62.

Meng, Y., Bian, L., Wang, Y., Lei, W., He, M., & Li, X. (2018). Global navigation augmentation system based on Hongyan satellite constellation. *Space International, 10*, 20–27.

Tian, S., Dai, W., Liu, R., Chang, J., & Li, G. (2014). System using hybrid LEO-GPS satellites for rapid resolution of integer cycle ambiguities. *IEEE Transactions on Aerospace and Electronic Systems, 50*(3), 1774–1785.

Tu, R., Ge, M., Zhang, H., & Huang, G. (2013). The realization and convergence analysis of combined PPP based on raw observation. *Advances in Space Research, 52*(1), 211–221.

Tu, R., Zhang, P., Zhang, R., Liu, J., & Lu, X. (2018). Modeling and assessment of precise time transfer by using BeiDou Navigation Satellite System triple-frequency signals. *Sensors, 18*(4).

Wright, T. J., Houlié, N., Hildyard, M., & Iwabuchi, T. (2012). Real-time, reliable magnitudes for large earthquakes from 1 Hz GPS precise point positioning: The 2011 Tohoku–Oki (Japan) earthquake. *Geophysical Research Letters*. https://doi.org/10.1029/2012GL051894

Wübbena, G., Schmitz, M., & Bagge, A. (2005). PPP-RTK: Precise point positioning using state-space representation in RTK networks. In *Proceedings of the 18th international technical meeting of the satellite division of the Institute of Navigation (ION GNSS 2005)* (pp. 2584–2594).

Xiao, G., Sui, L., Heck, B., Zeng, T., & Tian, Y. (2018). Estimating satellite phase fractional cycle biases based on Kalman filter. *GPS Solutions, 22*(3).

Zhang, X., & Andersen, O. B. (2006). Surface ice flow velocity and tide retrieval of the Amery ice shelf using precise point positioning. *Journal of Geodesy, 80*(4), 171–176.

Zhang, X., & Li, X. (2010). A new method for zero-differenced interger ambiguity resolution and its application to PPP. *Geomatics and Information Science of Wuhan University, 35*(6), 657–660.

Zhang, X., & Li, P. (2013). Assessment of correct fixing rate for precise point positioning ambiguity resolution on a global scale. *Journal of Geodesy, 87*(6).

Zhang, B., Teunissen, P. J. G., & Odijk, D. (2010). A novel undifferenced PPP-RTK concept. *Journal of Navigation, 64*(S1), S180-5191.

Zhang, B., Hou, P., Zha, J., & Liu, T. (2022a). PPP-RTK functional models formulated with undifferenced and uncombined GNSS observations. *Satellite Navigation, 3*(1).

Zhang, B., Ke, C., Zha, J., Hou, P., Liu, T., Yuan, Y., & Li, Z. (2022b). Undifferenced and uncombined PPP-RTK: Algorithmic models, prototype terminals and field-test results. *Acta Geodaetica Et Cartographica Sinica, 51*(8), 1725–1735.

Zhao, Q., Pan, S., Gao, C., Gao, W., & Xia, Y. (2020). BDS/GPS/LEO triple-frequency uncombined precise point positioning and its performance in harsh environments. *Measurement, 151*(3).

Zumberge, J. F., Heflin, M. B., Jefferson, D. C., Watkins, M. M., & Webb, F. H. (1997). Precise point positioning for the efficient and robust analysis of GPS data from large networks. *Journal of Geophysical Research: Solid Earth, 102*(B3), 5005–5017.

## Publisher's Note